Two-segment bistability and basin structure in three-segment PWL circuits

V. Špány
L. Pivka

Indexing terms: Piecewise-linear circuits, Bistability, Digital circuits

Abstract: Of all the piecewise-linear circuits known so far which exhibit two stable states, it is typical that their resistor characteristics each have at least three segments. The paper shows that bistability cannot be achieved via a two-segment characteristic in the plane. On the other hand, complicated bistable behaviour, including chaotic attractors, can occur locally at the boundary of two linear regions in higher-dimensional circuits. By using a three-segment characteristic, at least three attractors can be generated in the planar Lienard oscillator and five attractors are exhibited in three-dimensional Chua's circuit. Basin structure of the corresponding attractors is examined using numerical simulations. The use of basin delineation in the triggering of multistable circuits is shown.

1 Introduction

For several decades, from the very beginning of digital electronics, all textbooks and research works have been describing structures, capable of storing elementary 1-bit information, with resistors whose characteristics are approximated by at least three linear segments. We show that the number of segments necessary to achieve bistability has not yet been minimised.

Piecewise-linear (PWL) systems are being widely studied today from various aspects. For instance, two-segment idealised resistor characteristics have been used in synthetising Lorenz-type dynamics in circuits [1]. Discontinuous three-segment characteristics are considered in modelling multivibrators [2], while continuous symmetric three-region vector fields are treated in, among others, References 3 and 4. Our main concern will be to investigate the number and character of steady states, especially the number of attractors, in circuits governed by two- and three-region continuous vector fields.

The term bistability, here in its broader sense, will comprise situations when the two steady states can be arbitrary attractors, e.g. stable fixed points, limit cycles or chaotic attractors. In Section 2 we show that classical two-point bistability cannot arise in any dimension by patching up two linear vector fields continuously. An oscillatory type of bistability, however, is possible in dimensions greater than two as demonstrated in Section 4.

A most flexible and at the same time very simple circuit for investigating dynamic properties of multistable systems is Chua's circuit which was used as a chaos generator [5]. The circuit in Fig. 1 is described by the system

$$\begin{aligned} C_1(dv_1/dt) &= G(v_2 - v_1) - g(v_1) - I \\ C_2(dv_2/dt) &= G(v_1 - v_2) + i \\ L(di/dt) &= -v_2 \end{aligned} \tag{1}$$

where $g(v_1)$ is the PWL resistor characteristic and $G = 1/R$.

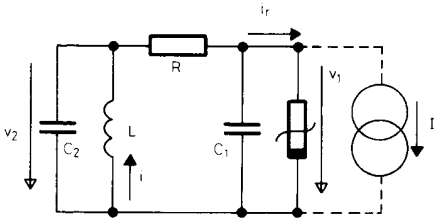

Fig. 1 *Circuit associated with system defined by eqn. 1*

The number and character of the steady states for eqn. 1 depends on the choice of the circuit parameters as will be shown in the following Sections.

2 General two-region continuous vector fields

The most widely used and simplest PWL vector fields are those which create linear 'layers'. More precisely we state the following.

Definition: Let $n \geq 1$, $r \geq 2$ be integers. Denote by L_r^n the class of all continuous vector fields f: $R^n \to R^n$ with the following property: there exist mutually parallel hyperplanes h_i $(i = 1, \ldots, r-1)$ dividing R^n into r regions $\mathscr{R}_i$ such that each restriction $f/\mathscr{R}_i$ $(i = 1, \ldots, r)$ can be extended to a linear vector field f_i on the whole of R^n. We shall write $f = (f_1, \ldots, f_r)$.

We focus our attention on the case $r = 2$. First we prove:

Proposition 1: Each $f \in L_2^n$ $(n \geq 1)$ can have at most one sink.

Proof: Assume the contrary, i.e. $f = (f_1, f_2) \in L_2^n$ having two sinks $\boldsymbol{P}$, $\bar{\boldsymbol{P}}$. Write $f_1(\boldsymbol{x}) = \boldsymbol{A}\boldsymbol{x} + \boldsymbol{b}$, $f_2(\boldsymbol{x}) = \bar{\boldsymbol{A}}\boldsymbol{x} + \bar{\boldsymbol{b}}$, where $\boldsymbol{A} = (a_{ij})$, $\bar{\boldsymbol{A}} = (\bar{a}_{ij})$ are matrices and $\boldsymbol{b}$, $\bar{\boldsymbol{b}}$ are vectors of dimension n. Without loss of generality we may

Paper 8893G (E10), received 10th February 1992

V. Špány is with the Department of Radio Electronics, Košice Institute of Technology, Park Komenského 13, 041 20 Košice, Czechoslovakia
L. Pivka is with the Computer Centre, Košice Institute of Technology, B. Němcovej 3, 042 00 Košice, Czechoslovakia

assume $h_1 = \{\boldsymbol{x} = [x_1, \ldots, x_n] \mid x_1 = 0\}$, so that $\boldsymbol{f}_1(\boldsymbol{x})$ and $\boldsymbol{f}_2(\boldsymbol{x})$ coincide if $x_1 = 0$. Then

$$a_{i2}x_2 + a_{i3}x_3 + \cdots + a_{in}x_n + b_i = \bar{a}_{i2}x_2 + \bar{a}_{i3}x_3 + \cdots + \bar{a}_{in}x_n + \bar{b}_i$$

for every $i = 1, 2, \ldots, n$ and for arbitrary choice of $x_2, x_3, \ldots, x_n$. Necessarily $\boldsymbol{b} = \bar{\boldsymbol{b}}$ and $a_{ij} = \bar{a}_{ij}$ for all $1 \leqslant i \leqslant n$, $2 \leqslant j \leqslant n$. Denote as $\boldsymbol{A}^{\boldsymbol{b}}$, $\bar{\boldsymbol{A}}^{\boldsymbol{b}}$ the matrices obtained, respectively, from $\boldsymbol{A}$, $\bar{\boldsymbol{A}}$ by replacing their first column with vector $-\boldsymbol{b}$. The first co-ordinates of $\boldsymbol{P}$, $\bar{\boldsymbol{P}}$ can then be expressed as

$$x_1^{\boldsymbol{P}} = \det \boldsymbol{A}^{\boldsymbol{b}}/\det \boldsymbol{A} \quad x_1^{\bar{\boldsymbol{P}}} = \det \bar{\boldsymbol{A}}^{\boldsymbol{b}}/\det \bar{\boldsymbol{A}}$$

by the Cramer rule. From the earlier equalities, $\det \boldsymbol{A}^{\boldsymbol{b}} = \det \bar{\boldsymbol{A}}^{\boldsymbol{b}}$. Moreover $\operatorname{sign}(\det \boldsymbol{A}) = \operatorname{sign}(\det \bar{\boldsymbol{A}}) = +1$ or -1 according to whether n is even or odd (since the determinant of a matrix is the product of its eigenvalues and by assumption all real parts of the eigenvalues of $\boldsymbol{A}$, $\bar{\boldsymbol{A}}$ are negative). Hence $\operatorname{sign}(x_1^{\boldsymbol{P}}) = \operatorname{sign}(x_1^{\bar{\boldsymbol{P}}})$, i.e. both sinks $\boldsymbol{P}$, $\bar{\boldsymbol{P}}$ lie in the same halfspace cut out by h_1 — a contradiction.

We next concentrate on two-region planar vector fields. Let $\boldsymbol{f} = (\boldsymbol{f}_1, \boldsymbol{f}_2) \in L_2^2$ and let $\boldsymbol{A}$, $\bar{\boldsymbol{A}}$ stand for the Jacobian matrices of $\boldsymbol{f}_1$ and $\boldsymbol{f}_2$, respectively. The following lemma is a consequence of the Bendixson criterion [6].

Lemma: A necessary condition for a limit cycle to occur for $\boldsymbol{f}$ is that the product of the traces $(\operatorname{Tr} \boldsymbol{A})(\operatorname{Tr} \bar{\boldsymbol{A}})$ be non-positive.

It is intuitively obvious and not difficult to prove that for a periodic attractor or repeller to arise in an $\boldsymbol{f} \in L_2^2$ it is also necessary that one of the following obtains:

(*a*) both $\boldsymbol{f}_1$ and $\boldsymbol{f}_2$ are spiral-type

(*b*) $\boldsymbol{f}_1$ is saddle-type and $\boldsymbol{f}_2$ is spiral-type or vice versa.

In Appendix I of Reference 7 it is proved that two limit cycles cannot arise in case (*a*). Following the arguments there one can extend the result also to the case (*b*):

Theorem: At most one limit cycle can exist in the phase portrait of any $\boldsymbol{f} \in L_2^2$. Bistability cannot arise for any such vector field.

Outline of proof: Suppose $\boldsymbol{f}$ generates a limit cycle and $\boldsymbol{f} = (\boldsymbol{f}_1, \boldsymbol{f}_2)$ where $\boldsymbol{f}_1$ is spiral source-type and $\boldsymbol{f}_2$ is saddle-type. The proof for other combinations is similar. With a suitable choice of local section (e.g. a line segment through the source, parallel to the x_2 axis) for the Poincaré return map one can derive the formula [7]:

$$g'(\lambda) = \{\lambda/g(\lambda)\}\left\{\int_0^{T_1(\lambda)} \operatorname{Tr} \boldsymbol{A} + \int_0^{T_2(\lambda)} \operatorname{Tr} \bar{\boldsymbol{A}}\right\} \tag{2}$$

where λ is the x_2 co-ordinate of the initial condition in the local section for the Poincaré map, $g(\lambda)$ is the x_2 co-ordinate of the corresponding returned point and $T_1(\lambda)$, $T_2(\lambda)$ denote the amounts of time spent by the solution curve in the halfplanes governed, respectively, by $\boldsymbol{f}_1$ and $\boldsymbol{f}_2$. In a manner similar to that given in Reference 7, we can see that T_1 is a decreasing function of λ and T_2 is an increasing function of λ. By the lemma and our assumptions, $\operatorname{Tr} \boldsymbol{A} > 0$ and $\operatorname{Tr} \bar{\boldsymbol{A}} \leqslant 0$, whence, from eqn. 2, the derivative $g'(\lambda) = \{\lambda/g(\lambda)\}G(\lambda)$ with the function G decreasing in the whole domain of definition. Finally we introduce the function $F(\lambda) = g(\lambda)/\lambda$ and derive $F'(\lambda)$. Using the expression for $g'(\lambda)$ we obtain $F'(\lambda) = \{G(\lambda) - F^2(\lambda)\}/\{\lambda F(\lambda)\}$. Since G is decreasing, it follows [7] that F is decreasing too. Moreover there is $\varepsilon > 0$ such that $F(\lambda) = C > 1$ for every $\lambda \in (0, \varepsilon)$ and F is a strictly decreasing function of λ in the rest of the definition domain. The first part of the theorem is thus established because periodic orbits correspond to those λ for which $F(\lambda) = 1$. The second part also follows, using proposition 1 and the Poincaré-Bendixson theorem.

Employing the above theorem, we sum up the possible steady state combinations in two-region PWL vector fields.

Proposition 2: Suppose $\boldsymbol{f} \in L_2^2$ and let $\boldsymbol{P}_s$ and $\boldsymbol{P}_n$ denote, respectively, stable and nonstable equlibrium points; denote $\boldsymbol{C}_s$ and $\boldsymbol{C}_n$ similarly for limit cycles. Chaotic limit sets being excluded by the Poincaré-Bendixson theorem, only the following combinations of steady states for $\boldsymbol{f}$ are possible:

$\boldsymbol{P}_s$ or $\boldsymbol{P}_n$	for one steady state
$\boldsymbol{P}_s\boldsymbol{P}_n$, $\boldsymbol{P}_n\boldsymbol{P}_n$, $\boldsymbol{P}_s\boldsymbol{C}_n$ or $\boldsymbol{P}_n\boldsymbol{C}_s$	for two steady states
$\boldsymbol{P}_s\boldsymbol{P}_n\boldsymbol{C}_n$ or $\boldsymbol{P}_n\boldsymbol{P}_n\boldsymbol{C}_s$	for three steady states.

The actual existence and circuit realisation of some non-trivial combinations are demonstrated in Section 3.

3 Attractors in the three-segment Lienard oscillator

By omitting the capacitor branch C_2 in Fig. 1, the classical Lienard oscillator is obtained. Setting $I = 0$, $C_1 = L = 1$ and $v = v_1$, its dynamics are described by the generalised Lienard equations

$$\begin{aligned} dv/dt &= i - g(v) \\ di/dt &= -i/G - v \end{aligned} \tag{3}$$

Our objective is to observe the dynamics of eqn. 3 with three-segment PWL characteristic g passing through the origin. For the numerical simulation we chose the following parameter values:

$$\begin{aligned} G &= 1.6 \quad & m^- &= -0.25 \\ m &= -2.5 \quad & m^+ &= -0.25 \\ B^- &= -0.4 \quad & B^+ &= 0.4 \end{aligned} \tag{4}$$

Here m^-, m, m^+ are the slopes, respectively, of the left, centre and right segments of the characteristic g and $B^{\pm}$ are the breakpoints. We will observe the bifurcation phenomena by changing the slope m^+, while the other parameters in eqn. 4 remain constant. To facilitate explanation of the circuit dynamics, $\mathscr{B}(\boldsymbol{A})$ will denote the basin boundary for attractor $\boldsymbol{A}$, and $\alpha(T)$ and $\omega(T)$ will, respectively, stand for the α- and ω-limit sets of trajectory T.

The situation for the values in eqn. 4 is depicted in Fig. 2*a*. Three attractors are exhibited by the circuit: two stable stationary points $\boldsymbol{P}^{\pm}$, surrounded by unstable periodic orbits $\boldsymbol{C}_n^{\pm}$, and a stable limit cycle $\boldsymbol{C}_s$. Now let m^+ vary. For $m^+ \leqslant -1.6$ there is no fixed point in the halfplane $v > 0$, whereas for $-1.6 < m^+ < -0.89$ the equilibrium $\boldsymbol{P}^+$ is unstable: the circuit is monostable. Increasing m^+, a large stable orbit $\boldsymbol{C}_s$ is born at $m^+ \simeq -0.89$. An oscillatory flip-flop is thus formed. The value $m^+ = -0.625$ is a Hopf bifurcation point: $\boldsymbol{P}^+$ becomes a sink and an unstable limit cycle $\boldsymbol{C}_n^+$ appears around $\boldsymbol{P}^+$ — the circuit represents a triflop (Fig. 2*a*). Using the above notation we have $\mathscr{B}(\boldsymbol{P}^+) = \boldsymbol{C}_n^+$, $\mathscr{B}(\boldsymbol{P}^-) = \boldsymbol{C}_n^-$, $\mathscr{B}(\boldsymbol{C}_s) = \boldsymbol{C}_n^+ \cup \boldsymbol{C}_n^- \cup W^s(\boldsymbol{O})$, $\alpha\{W_+^s(\boldsymbol{O})\} = \boldsymbol{C}_n^+$, $\alpha\{W_-^s(\boldsymbol{O})\} = \boldsymbol{C}_n^-$, $\omega\{W_+^u(\boldsymbol{O})\} = \omega\{W_-^u(\boldsymbol{O})\} = \boldsymbol{C}_s$,

where $W^s(O)$, $W^u(O)$ [$W^s_\pm(O)$, $W^u_\pm(O)$] denote the stable and unstable [half] manifolds of the origin O.

This situation persists up to $m^+ \simeq -0.165$ when $W^s_+(O)$ and $W^u_+(O)$ merge to form a homoclinic orbit. Boundary $\mathscr{B}(P^+)$ changes and consists of the homoclinic $H \cup O \cup W^s_-(O)$, $\mathscr{B}(P^-) = C_n^-$, $\omega\{W^u_+(O)\} = P^+$, $\alpha\{W^s_-(O)\} = C_n^-$, $\omega\{W^s_+(O)\} = \omega\{W^u_-(O)\} = O$.

After the breakdown of the homoclinic at $m^+ > 0.21$ a triple of nested cycles is created through the appearance of the periodic repeller C_n (Fig. 2c), which is the bound-

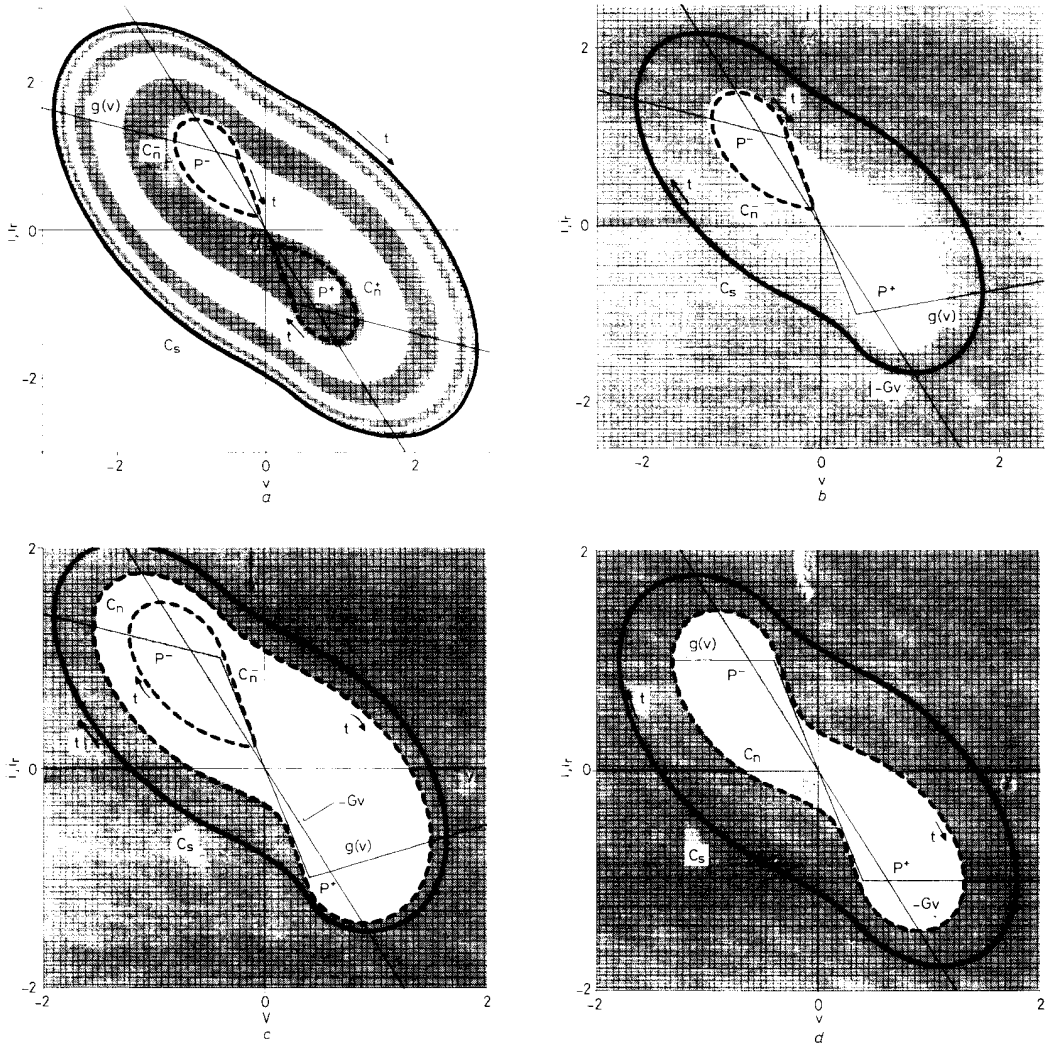

Fig. 2 *Bifurcations in Lienard's oscillator*

a Limit cycles for the triflop defined by parameter values in eqn. 4. The grey and white regions inside C_s represent the basins, in reverse time, for the orbits $C_n^\pm$
b Domains of attraction for C_s (dark grey), P^- (light grey) and P^+ (white) at $m^- = 0.18$
c Basin structure after breakdown of homoclinic, $m^+ = 0.3$
d Case of symmetric characteristic g at $m^\pm = 0$

and the origin. Since the vector field is structurally unstable at this point, the homoclinic breaks down immediately with a slightest increase in m^+. For $-0.165 < m^+ < 0.21$ the basin of P^+ wraps around C_n^- (see Fig. 2b) where $m^+ = 0.18$, $\mathscr{B}(P^+) = \mathscr{B}(C_s) = W^s(O) \cup C_n^-$, $\mathscr{B}(P^-) = \alpha\{W^s_-(O)\} = \alpha\{W^s_+(O)\} = C_n^-$ and $\omega\{W^u_+(O)\} = P^+$, $\omega\{W^u_-(O)\} = C_s$. Another homoclinic connection H occurs at $m^+ \simeq 0.21$, this time by flowing of $W^u_-(O)$ into $W^s_+(O)$. As a result, $\mathscr{B}(C_s) = H \cup O$, ary for the basin of C_s. Further, $\mathscr{B}(P^-) = C_n^-$, $\mathscr{B}(P^+) = C_n \cup C_n^- \cup W^s(O)$, $\alpha\{W^s_-(O)\} = C_n^-$, $\alpha\{W^s_+(O)\} = C_n$, $\omega\{W^u_+(O)\} = \omega\{W^u_-(O)\} = P^+$. Collision of C_n with C_s occurs at $m^+ \simeq 0.338$ resulting in the disappearance of C_s. The stable manifold $W^s(O)$ and the basin for P^+ become unbounded for every $m^+ > 0.338$: the circuit is a flip-flop.

We could have changed both slopes $m^\pm$ simultaneously and obtained a symmetric bifurcation scenario

similar to the above — see Fig. 2*d* for a symmetric choice of $m^{\pm} = 0$ with $\mathscr{B}(\boldsymbol{P}^+) = \mathscr{B}(\boldsymbol{P}^-) = W^s(\boldsymbol{O}) \cup \boldsymbol{C}_n$, $\mathscr{B}(\boldsymbol{C}_s) = \boldsymbol{C}_n$, $\alpha\{W^s_+(\boldsymbol{O})\} = \alpha\{W^s_-(\boldsymbol{O})\} = \boldsymbol{C}_n$, $\omega\{W^u_+(\boldsymbol{O})\} = \boldsymbol{P}^+$ and $\omega\{W^u_-(\boldsymbol{O})\} = \boldsymbol{P}^-$.

To end this Section, some remarks on realisability are in order. We wish to find parameter values such that various steady-state combinations of Proposition 2 (Section 2) are generated via two-segment characteristic g. The first four combinations are easy to realise and we have already seen that combination $\boldsymbol{P}_s\boldsymbol{P}_n\boldsymbol{C}_n$ can be generated setting $G = 1.6$, $m^- = -0.25$, $m = m^+ = -2.5$, $B^{\pm} = \pm 0.4$ (see Fig. 2). Combinations $\boldsymbol{P}_s\boldsymbol{C}_n$ and $\boldsymbol{P}_n\boldsymbol{C}_s$ are obtained, respectively, with $G = 2$, $m^- = m = 0.3$, $m^+ = -1.3$, $B^{\pm} = \pm 1$ and $G = 2$, $m^- = m = -1$, $m^+ = 1$, $B^{\pm} = \pm 1$. To find out why $\boldsymbol{P}_n\boldsymbol{P}_n\boldsymbol{C}_s$ is not realisable with $G > 0$ assume $f = (f_1, f_2) \in L^2_2$ is generated by eqn. 3 where $m^- = m$, f_1 is saddle-type and f_2 is spiral-type. Let $\boldsymbol{A}$ and $\bar{\boldsymbol{A}}$ denote, respectively the Jacobian matrices for f_1 and f_2. Then $\mathrm{Tr}\,\boldsymbol{A} = -m - 1/G$, $\mathrm{Tr}\,\bar{\boldsymbol{A}} = -m^+ - 1/G$, $\det \boldsymbol{A} = -m/G + 1$ and $\det \bar{\boldsymbol{A}} = -m^+/G + 1$. By the hypothesis on f_1, f_2: $\det \boldsymbol{A} < 0 < \det \bar{\boldsymbol{A}}$. From the Lemma of Section 2 $\mathrm{Tr}\,\boldsymbol{A} < 0 < \mathrm{Tr}\,\bar{\boldsymbol{A}}$ if $\boldsymbol{C}_s$ exists. The two left-hand inequalities yield $-1/G < m < -G$, while the two right-hand inequalities give $-G < m^+ < -1/G$ which cannot be met at the same time. Therefore combination $\boldsymbol{P}_n\boldsymbol{P}_n\boldsymbol{C}_s$ is only realisable with (synthesised) negative conductances, e.g. with $G = -1.3$, $m^- = m = 2.5$, $m^+ = 0.7$, $B^{\pm} = \pm 1$. Thus, via two segments and G arbitrary, the circuit is capable of realising any combination of Proposition 2.

4 Two-segment bistability

Having explored the vector field classes L^2_2 and L^2_3 we move on to the more complex three-dimensional circuits. In contrast to L^2_r the situation is further complicated by the appearance of chaotic attractors in vector fields of class L^3_r. In Section 2 it was proved that vector fields from L^n_2 do not give rise to bistability if $n = 2$. For $n \geqslant 3$, however, this is no longer true.

Consider the system of eqn. 1 where the characteristic g has two segments with slopes m^-, m and the breakpoint B^-. On the basis of the information contained in Reference 7 the parameters for the two-dimensional circuit, obtained from Fig. 1 by letting $C_2 \to 0$, were chosen so as to satisfy the conditions for existence of a nonstable limit cycle $\boldsymbol{C}_n^-$. The periodic orbit is also present in the three-dimensional circuit of Fig. 1 at the following parameter values

$$1/C_1 = 8 \quad 1/C_2 = 1 \quad 1/L = 7 \quad G = 0.7 \tag{5}$$
$$m^- = -0.1 \quad m = -0.8 \quad B^- = -1 \quad I = 0$$

Computer simulation revealed, however, that a stable limit cycle $\boldsymbol{C}_s^-$ coexists in a close neighbourhood of the saddle-type periodic orbit $\boldsymbol{C}_n^-$. This is quite remarkable since balance between the contractive force of the halfspace $v_1 < B^-$ and the expansive force of the halfspace $v_1 > B^-$ is reached at two different locations.

At the parameter values (eqn. 5) the co-ordinates of the stable fixed point $\boldsymbol{P}^-$ are $v_1 \simeq -1.167$, $v_2 = 0$, $i \simeq 0.817$ and the eigenvalues of the Jacobian matrix at the origin $\boldsymbol{O}$ were computed to be $\lambda_1 \simeq 1.3396$, $\lambda_{2,3} \simeq -0.618 \pm j1.9484$, while those at $\boldsymbol{P}^-$ were $\mu_1 \simeq -5.45$, $\mu_{2,3} \simeq -0.0252 \pm j2.483$. The nonstable periodic orbit $\boldsymbol{C}_n^-$ is a saddle-type source (in backward time) of the trajectories defining the boundary surface $W^s(\boldsymbol{C}_n^-)$ that separates the domains of attraction for $\boldsymbol{P}^-$ and $\boldsymbol{C}_s^-$. Some techniques for graphical representation of boundary surfaces and basins, applied to Chua's circuit, are illustrated in Reference 8. Here we use the grid technique to delineate the basins of attraction for $\boldsymbol{C}_s^-$ and $\boldsymbol{P}^-$. In Fig. 3*a* the green–orange and the black-orange boundaries define the cross-sections of boundary surfaces $W^s(\boldsymbol{C}_n^-)$ and $W^s(\boldsymbol{O})$ respectively. The basin boundaries for the two attractors are $\mathscr{B}(\boldsymbol{P}^-) = W^s(\boldsymbol{C}_n^-) \cup W^s(\boldsymbol{O})$ and $\mathscr{B}(\boldsymbol{C}_s^-) = W^s(\boldsymbol{C}_n^-)$. Of course the stable manifold $W^s(\boldsymbol{O})$ is linear in a close neighbourhood of the origin since it coincides there with the stable eigenspace $E^s(\boldsymbol{O})$.

5 Basin structure in three-segment Chua's circuit

We now examine the appearance of steady states, attractors and the corresponding basin structure bifurcations in the system defined by eqn. 1 with three-segment characteristic g. By analogy with Section 3, the slope m^+ of the right-hand segment will serve as the bifurcation parameter.

5.1 From flip-flop to pentaflop

With the parameter set (eqn. 5) and $m^+ \leqslant -0.7$, $B^+ = 1$, the circuit is a flip-flop model described in the preceding Section. Another equilibrium point $\boldsymbol{P}^+$ appears for $-0.7 < m^+ < -0.607$ which is a sink. This can be verified, for example, by applying the Routh stability criterion [10]; see also the Appendix in Reference 11. Thus the circuit represents a triflop whose phase portrait is very much like that of Fig. 3*a*, the difference being that the black region is the domain of attraction for the sink $\boldsymbol{P}^+$, and $\mathscr{B}(\boldsymbol{P}^+) = W^s(\boldsymbol{O})$. A Hopf bifurcation at $m^+ \simeq -0.607$ signifies the birth of not only the stable orbit $\boldsymbol{C}_s^+$ around $\boldsymbol{P}^+$ but also of a large saddle-type orbit $\boldsymbol{C}_n$. Despite the emergence of $\boldsymbol{C}_s^+$, the circuit remains tristable, because $\boldsymbol{P}^+$ loses its stability. In Fig. 3*b* $m^+ = -0.4$ with $\mathscr{B}(\boldsymbol{P}^-) = W^s(\boldsymbol{C}_n^-) \cup W^s(\boldsymbol{O}) \cup W^s(\boldsymbol{C}_n)$, $\mathscr{B}(\boldsymbol{C}_s^-) = W^s(\boldsymbol{C}_n^-) \cup W^s(\boldsymbol{C}_n)$, $\mathscr{B}(\boldsymbol{C}_s^+) = \boldsymbol{P}^+ \cup W^s(\boldsymbol{O}) \cup W^s(\boldsymbol{C}_n)$. Note the tabular shape of the unbounded stable manifold $W^s(\boldsymbol{C}_n)$ which separates those initial conditions that are attracted toward $\boldsymbol{P}^-$, $\boldsymbol{C}_s^-$ or $\boldsymbol{C}_s^+$ from those which diverge. Compare this with the question about the behaviour of $W^s(\boldsymbol{C}_n)$ raised in Reference 5, pp. 802–803. For a more thorough treatment of the question refer to References 8 and 9. If $m^+ > -0.24$ the divergent trajectories of the system become convergent, namely toward a large stable periodic attractor $\boldsymbol{C}_s$ encircling the tube $W^s(\boldsymbol{C}_n)$. Thus the circuit is a tetraflop in the interval $-0.24 < m^+ < -0.18$. At $m^+ \simeq -0.18$ the equilibrium point $\boldsymbol{P}^+$ regains its stability, thus adding one more attractor to the system. The domains of attraction in the odd-symmetric pentaflop circuit with $m^+ = -0.1$ are depicted in Fig. 3*c* and *d*. The large stable limit cycle $\boldsymbol{C}_s$ is not visible because of its great size. Altogether, the total number of equilibrium solutions is nine: six periodic orbits along with three fixed points. The five attractors survive until $m^+ \simeq -0.05$ at which value the orbit $\boldsymbol{C}_s^+$ disappears and the phase portrait is similar to Fig. 3*b*. Another attractor is lost if we increase the slope to $m^+ = 1.25$, when $\boldsymbol{C}_n$ and $\boldsymbol{C}_s$ grow together and disappear. The remaining three attractors $\boldsymbol{P}^{\pm}$, $\boldsymbol{C}_s$ keep their stability for all $m^+ > 1.25$. Fig. 3*e* shows the situation with $m^+ = 5$.

5.2 Other 1-parameter bifurcation phenomena

Some additional bifurcations can be observed from Chua's circuit if we change parameters other than m^+ while keeping the remaining ones fixed. It turns out that, even if the zeros $\boldsymbol{P}^{\pm}$ are sinks, the circuit can be chaotic, although we did not observe the double-scroll structure

[5]. In what follows we assume the basic set of parameters is chosen as in eqn. 5 with $m^+ = m^- = -0.1$ and $B^+ = 1$, (i.e. symmetric three-segment characteristic g).

5.2.1 Capacitance bifurcations

Let $1/C_1$ vary. For $0 < 1/C_1 < 7$ the equilibria $P^{\pm}$ are sinks and no periodic motion can be observed. In the

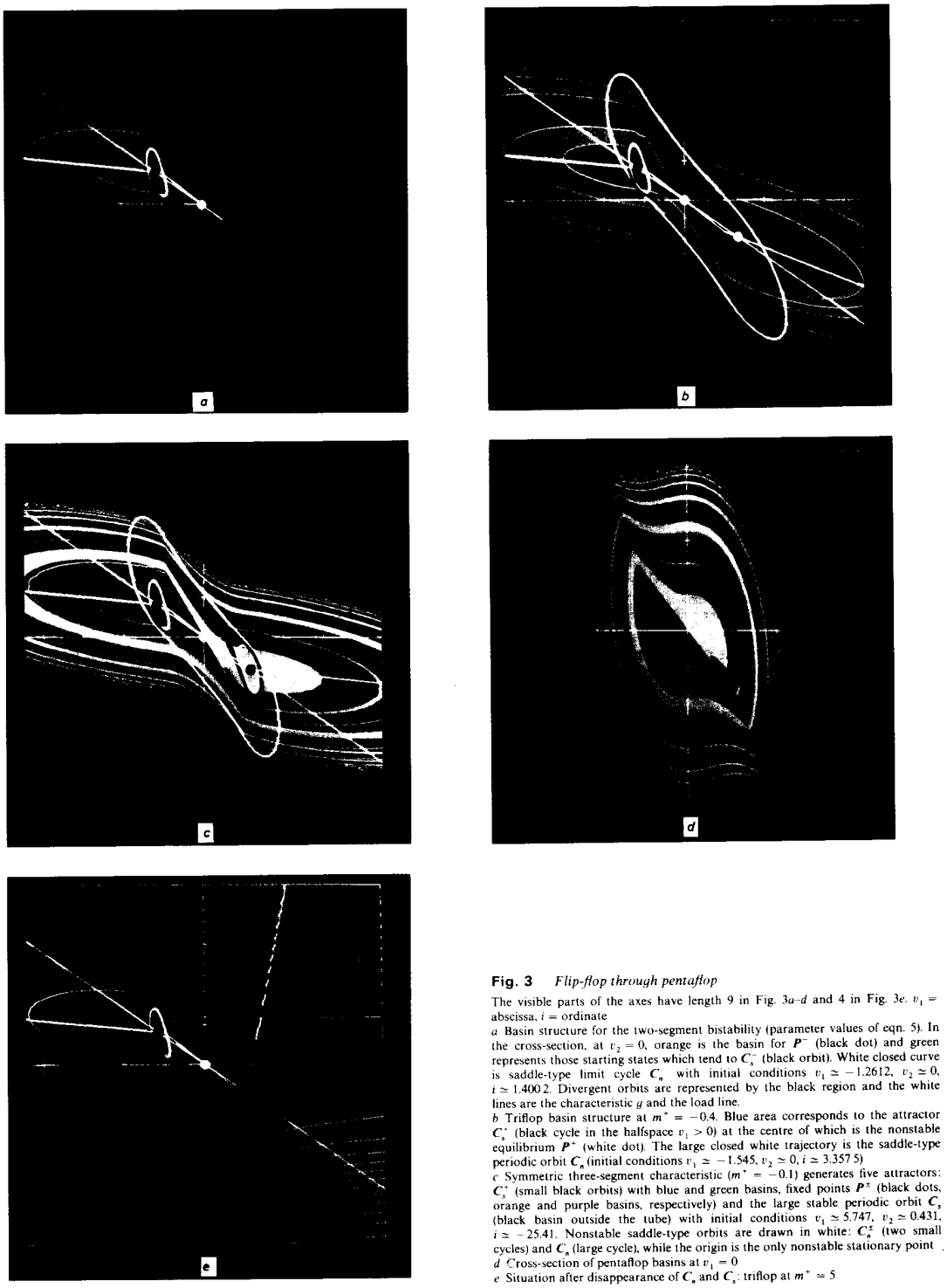

Fig. 3 *Flip-flop through pentaflop*

The visible parts of the axes have length 9 in Fig. 3*a–d* and 4 in Fig. 3*e*. v_1 = abscissa, i = ordinate

a Basin structure for the two-segment bistability (parameter values of eqn. 5). In the cross-section, at $v_2 = 0$, orange is the basin for P^- (black dot) and green represents those starting states which tend to C_s^- (black orbit). White closed curve is saddle-type limit cycle C_n with initial conditions $v_1 \simeq -1.2612$, $v_2 \simeq 0$, $i \simeq 1.4002$. Divergent orbits are represented by the black region and the white lines are the characteristic g and the load line.

b Triflop basin structure at $m^* = -0.4$. Blue area corresponds to the attractor C_s^* (black cycle in the halfspace $v_1 > 0$) at the centre of which is the nonstable equilibrium P^* (white dot). The large closed white trajectory is the saddle-type periodic orbit C_n (initial conditions $v_1 \simeq -1.545$, $v_2 \simeq 0$, $i \simeq 3.3575$)

c Symmetric three-segment characteristic ($m^* = -0.1$) generates five attractors: C_s^* (small black orbits) with blue and green basins, fixed points $P^{\pm}$ (black dots, orange and purple basins, respectively) and the large stable periodic orbit C_s (black basin outside the tube) with initial conditions $v_1 \simeq 5.747$, $v_2 \simeq 0.431$, $i \simeq -25.41$. Nonstable saddle-type orbits are drawn in white: $C_n^{\pm}$ (two small cycles) and C_n (large cycle), while the origin is the only nonstable stationary point

d Cross-section of pentaflop basins at $v_1 = 0$

e Situation after disappearance of C_n and C_s: triflop at $m^+ = 5$

interval $7 < 1/C_1 < 7.7$ a large stable cycle C_s is present, so that the circuit represents a triflop. At $1/C_1 \simeq 7.7$ a period-doubling cascade is initiated: period-1 for $7.7 < 1/C_1 < 9.05$, period-2 for $9.05 < 1/C_1 < 9.29$, period-4 if $9.29 < 1/C_1 < 9.35$ etc. Finally the circuit becomes chaotic, and a pair of Rössler's spiral-type attractors are born around $P^{\pm}$ (Fig. 4; see also Reference 11 where the zeros $P^{\pm}$ are nonstable). The circuit has a pentaflop

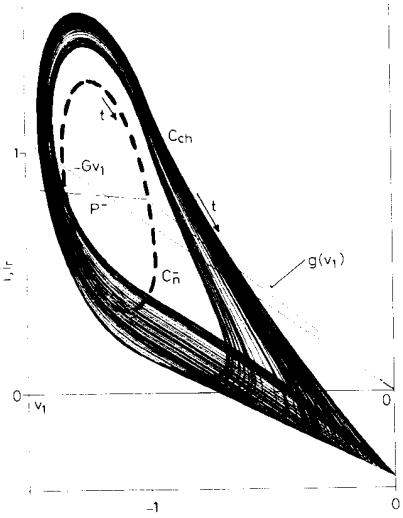

Fig. 4 *Rössler's spiral-type attractor at $1/C_1 = 9.5$*
Broken line is projection of saddle-type limit cycle C_n^- (initial conditions $v_1 \simeq -1.2389$, $v_2 \simeq 0$, $i \simeq 1.2908$) encircling the stable equilibrium P^-

structure analogous to that of Section 5.1. The Rössler's attractors persist at least for $9.38 < 1/C_1 < 9.7$. With a further increase in $1/C_1$, instead of merging to form a double-scroll attractor, these attractors seem to disappear — the system is tristable with $P^{\pm}$ and C_s for its attractors. The equilibria $P^{\pm}$ lose their stability and C_s vanishes at $1/C_{1s} \simeq 10.22$.

5.2.2 C_2 bifurcations

Here a similar bifurcation scenario can be observed as with C_1, but the equilibria $P^{\pm}$ lose their stability *en route* to chaos. $P^{\pm}$ are sinks for $1/C_2 > 1.1$. In the interval $0.69 < 1/C_2 < 1.1$ period-1 orbits are present around $P^{\pm}$. These orbits bifurcate into period-2 orbits which persist for $0.62 < 1/C_2 < 0.68$. The equilibria $P^{\pm}$ become nonstable at around $1/C_2 \simeq 0.59$ which value falls within the period-4 interval. If $1/C_2$ is decreased further, Rössler's (at, for example $1/C_2 = 0.55$) and the double scroll attractor ($1/C_2 = 0.35$) can be observed.

6 Switching in multistable PWL circuits

When investigating a sequential circuit it is often a matter of practical importance to know how to switch among its stable steady states. In the flip-flop circuit of Section 4 this can be achieved, for example, by using the conductance G as the switching parameter: at $G = 0.3$ and $G = 0.5$, the equilibrium P^- is the only attractor of the circuit, lying in the basin of P^- and of C_s, respectively, for the original set of circuit parameters (eqn. 5). By varying G for appropriate time periods one can switch between the attractors P^- and C_s. In some other situations, trigger pulse I (Fig. 1) can be used for the purposes of switching. By way of illustration, consider the triflop from Section 5.1 at $m^+ = 1$. For each of the pulse values $I = 0.8$, $I = -2$ and $I = 0.3$, the circuit is monostable with the corresponding sinks P_1, P_2, P_3 lying on the load line (Fig. 5). Let the starting point be P^- at $I = 0$.

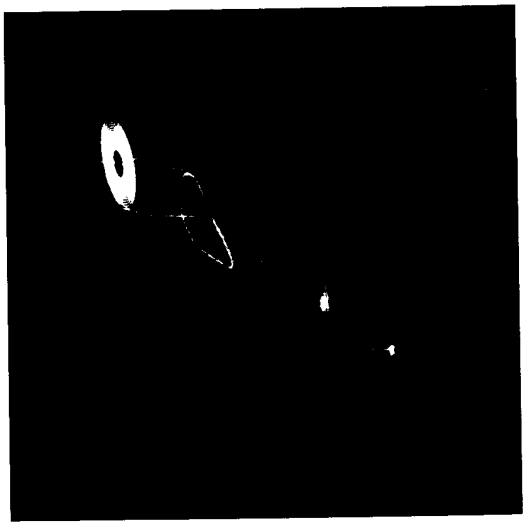

Fig. 5 *Trajectory of switching process in the triflop at $m^+ = 1$*
White and green broken lines are characteristics shifted by pulse height $I = 0.8$ and $I = -2$, respectively.

Then applying successively the pulses $I = 0.8$ of width $W(I) = 50$ (white trajectory), $I = 0$ with $W(I) = 20$ (yellow), $I = -2$ with $W(I) = 20$ (green), $I = 0$ with $W(I) = 20$ (purple), $I = 0.3$ with $W(I) = 50$ (not shown in Fig. 5 to avoid clutter) and $I = 0$ with $W(I) = 50$, the switching sequence

$$P^- \rightarrow P_1 \rightarrow C_s^- \rightarrow P_2 \rightarrow P^+ \rightarrow P_3 \rightarrow P^-$$

is realised.

In these, as in many other cases, cross-sections of basins can be utilised in estimating the appropriate slope of the load line or the height of the pulse needed to achieve the triggering effect. For more information on the control of memory cells, see References 8, 12 and 13.

7 Concluding remarks

The two-segment bistability minimises the number of segments necessary to generate two attractors with the PWL type of nonlinearity. Employing symmetry, this permits the generation of as many as five attractors by using only three-segment approximation to the nonlinear element.

In the chaotic systems investigated so far, all the equilibrium points involved were nonstable. This need not always be the case, however, as shown in Section 5.2.1.

We have seen in the last Section how computer-generated cross-sections of basins can be exploited in the estimation of switching parameters. The associated boundary surfaces make it possible to find out the parameters of the critical control pulses (the pulses at which the trajectory reaches the boundary surface). In such a way, an in-depth analysis of problems connected with metastability [14] will be possible, and answers to questions regarding unstable states of flip-flop sensors [15] can be given.

8 References

1 TOKUNAGA, R., KOMURO, M., and CHUA, L.O.: '"Lorenz attractor" from an electrical circuit with uncoupled continuous piecewise-linear resistor', *Int. J. Circuit Theory Appl.*, 1989, **17**, (1), pp. 71–85

2 VASILJEVIĆ, D.M.: 'Nonlinear analysis of a quartz multivibrator with a complementary switch', *IEE Proc. G. Electron. Circuits & Syst.*, 1985, **132**, (2), pp. 33–38

3 CHUA, L.O., KOMURO, M., and MATSUMOTO, T.: 'The double scroll family', *IEEE Trans.*, 1986, **CAS-33**, (11), pp. 1073–1118

4 CHUA, L.O., and LIN, G.-N.: 'Canonical realization of Chua's circuit family', *IEEE Trans.*, 1990, **CAS-37**, (7), pp. 885–902

5 MATSUMOTO, T., CHUA, L.O., and KOMURO, M.: 'The double scroll', *IEEE Trans.*, 1985, **CAS-32**, (8), pp. 798–818

6 ANDRONOV, A.A., WITT, A., and KHAIKIN, S.E.: 'Theory of oscillations' (Addison Wesley, 1966)

7 FLATTO, L.: 'Limit cycle studies for circuits containing one Esaki diode', *J. Math. Anal. Appl.*, 1964, **9**, (3), pp. 360–383

8 ŠPÁNY, V., and PIVKA, L.: 'Boundary surfaces in sequential circuits', *Int. J. Circuit Theory Appl.*, 1990, **18**, (4), pp. 349–360

9 ŠPÁNY, V., and PIVKA, L.: 'Invariant manifolds and generation of chaos', *Elektrotechnický časopis*, 1988, **39**, (6), pp. 417–431

10 ROUTH, E.J.: 'Dynamics of a system of rigid bodies' (Macmillan, 1905)

11 MATSUMOTO, T., CHUA, L.O., and KOMURO, M.: 'The double scroll bifurcations', *Int. J. Circuit Theory Appl.*, 1986, **14**, (2), pp. 117–146

12 ŠPÁNY, V., and PIVKA, L.: 'Boundary surfaces in sequential circuits', *in* 'Contributions to the Theory of Electrical Engineering'. International Symposium on Theoretical Electronics, Ilmenau, 1988, pp. 90–99

13 ŠPÁNY, V.: 'Computer simulation of dynamical properties of a memory cell' (in Slovak), *Elektrotechnický časopis*, 1987, **38**, (8), pp. 585–608

14 KIM, L.S., and DUTTON, R.W.: 'Metastability of CMOS latch/flip-flop', *IEEE J. Solid-state Circuits*, 1990, **25**, (4), pp. 942–951

15 LIAN, W.J., and MIDDELHOEK, S.: 'A new class of integrated sensors with digital output based upon the use of a flip-flop', *IEEE Electron Device Lett.*, 1986, **EDL-7**, (4), pp. 238–240